PHYSICS OF FLUIDS **26**, 096604 (2014)

Internal wave energy radiated from a turbulent mixed layer

James R. Munroe[1,a)] and Bruce R. Sutherland[2,b)]
[1]*Department of Physics and Physical Oceanography, Memorial University of Newfoundland, St. John's, Newfoundland A1B 3X7, Canada*
[2]*Departments of Physics and Earth and Atmospheric Sciences, University of Alberta, Edmonton, Alberta T6G 2R3, Canada*

(Received 18 July 2014; accepted 2 September 2014; published online 17 September 2014)

We examine mixed-layer deepening and the generation of internal waves in stratified fluid resulting from turbulence that develops in response to an applied surface stress. In laboratory experiments the stress is applied over the breadth of a finite-length tank by a moving roughened conveyor belt. The turbulence in the shear layer is characterized using particle image velocimetry to measure the kinetic energy density. The internal waves are measured using synthetic schlieren to determine their amplitudes, frequencies, and energy density. We also perform fully nonlinear numerical simulations restricted to two dimensions but in a horizontally periodic domain. These clearly demonstrate that internal waves are generated by transient eddies at the integral length scale of turbulence and which translate with the background shear along the base of the mixed layer. In both experiments and simulations we find that the energy density of the generated waves is 1%–3% of the turbulent kinetic energy density of the turbulent layer. © *2014 AIP Publishing LLC*. [http://dx.doi.org/10.1063/1.4895645]

I. INTRODUCTION

Internal waves move within a density stratified fluid under the influence of buoyancy forces. In the ocean, the waves are understood to act as a conduit through which large scale disturbances, such as storms acting on the surface or the barotropic tide acting on bottom topography, transport their energy to the ocean interior and, through breaking, transfer their energy to small-scale turbulence and mixing. In this paper we consider the inverse process whereby turbulence excites internal waves. Specifically we are concerned with the process in which eddies in a turbulent shear flow interact with the underlying thermocline to create internal waves. While this wave radiation may not significantly change the dynamics of the turbulent layer,[1] the cumulative excitation of waves beneath the wind-driven ocean mixed layer may serve as an important source of energy that can mix the deeper ocean.

There have been a growing number of experimental and numerical investigations of turbulence-generated internal waves. In some of these the turbulence results from solid objects as in the wake behind a towed sphere[2,3] or a tall obstacle,[4] turbulence above and in the lee of flow over rough topography,[5] and an oscillatory turbulent patch surrounding large amplitude oscillations of a cylinder.[6] Internal waves have also been observed[7] and measured[8] in mixing box experiments where statistically stationary turbulence results from a vertically oscillating horizontal grid of bars overlying a stratified region. Conical internal waves have also been observed to emanate from the top of a fountain impinging in a stratified fluid,[9] consistent with observations of mesospheric internal waves generated by a thunderstorm.[10] Numerical simulations have also revealed internal waves being generated by unstable shear flows in non-uniformly stratified fluid[11–14] by a turbulent Ekman layer[15] and by a turbulent boundary layer associated with tidal flow over a slope.[16]

a)URL: http://www.physics.mun.ca/~jmunroe; jmunroe@mun.ca.
b)URL: http://www.ualberta.ca/~bsuther; bsuther@ualberta.ca.

Remarkably, in all these circumstances in which waves were excited by fully three-dimensional turbulence, the wave frequency, ω, relative to the buoyancy frequency, N, was found to lie within a narrow range about $\omega/N \approx 0.7$, corresponding to waves whose constant-phase lines tilt at 45° to the vertical. In the case of the turbulent Ekman layer, Taylor and Sarkar[15] showed this to be the result of selective filtering whereby waves with slower vertical group speed were viscously damped closer to the source. However, in laboratory experiments[4–6,8,9] and in simulations of the wake behind a towed sphere[3] the narrow bandedness was evident adjacent to the source itself. It has been hypothesized[8] that this frequency-selection is a consequence of a weakly nonlinear feedback between the waves and turbulent eddies adjacent to the stratified fluid: waves that propagate at 45° transport the greatest momentum and so exert the most drag on the source.

From laboratory experiments that measure the energy associated with turbulence-generated waves, another common observation is that the vertical displacement amplitude of the waves is 2%–5% of their horizontal wavelength. This is in the range of amplitudes for which nonhydrostatic internal waves are considered to be weakly nonlinear.[17,18]

In the experiments reported upon here we examine the properties of internal waves generated by an obstacle-free turbulent shear flow. In this way we are able to assess more directly the efficiency by which wind-generated surface mixing may impart energy into the thermocline via internal waves.

Specifically we apply a surface stress over an initially uniformly stratified fluid and we examine the properties of the resulting turbulent shear flow and the internal waves it generates in the relatively quiescent fluid beneath. Conceptually, the experimental setup is similar to that of Kato and Phillips,[19] although their experiments were performed in an annular tank and their analysis focused upon the deepening of the mixed layer, not internal waves. Our experiments are performed in a finite-length tank leading to a more complex circulation in the mixed region: for a rightward applied stress, there was a mean rightward surface flow and leftward counter current. Because the process of wave-generation takes place at the interface between the turbulent and stratified region, the details of the circulation pattern far above the interface should not influence wave-generation except insofar as it influences the structure of eddies at the integral length scale of the turbulence. This is corroborated by the results of numerical simulations performed in a horizontally periodic domain. Another advantage of our setup being in a rectangular tank is that the turbulence and internal waves are not influenced by centripetal forces associated with flow around an annulus.

In Sec. II, we describe the setup, analysis methods, and results of the laboratory experiments. First we briefly examine the descent of the interface due to turbulent entrainment and we compare the results to those of other experiments that have examined mixed-layer deepening. We then examine the mean and fluctuating flow in the turbulent field and we examine the properties of underlying internal waves. We were primarily interested in determining the fraction of energy of the turbulent mixed layer that radiates away as internal waves. Section III presents direct numerical simulations that model and extend the laboratory results from the conveyor belt experiment. The two-dimensional simulations in a horizontally periodic domain show the same qualitative features as the laboratory experiments suggesting that the generation of internal waves in sheared turbulence is essentially a two-dimensional mechanism and the presence of tank end walls is not critical to the energetics of the wave generation. Implications of this work are discussed in Sec. IV.

II. LABORATORY EXPERIMENTS

In this section we describe the set-up and results of laboratory experiments examining mixed-layer deepening and internal wave generation by a turbulent shear flow resulting from an imposed surface stress. Although designed to model an idealization of a wind stress applied to the surface of a stratified ocean, because the tank had finite length, the surface forcing resulted in a circulation with fluid moving in the direction of the stress near the surface and moving in the opposite direction beneath, but still within the mixed region. This turbulent return flow gradually entrained the underlying stratified fluid while simultaneously eddies impinging upon the stratified fluid launched internal waves. While we briefly examine the entrainment velocity, the focus of this study is upon internal wave generation. An advantage of this experimental set-up was that on the time scale of the buoyancy period, the amount of energy in the turbulent mixed layer and lower stratified mixed layer

was in quasi-steady state, allowing time averages to be calculated. Our primary goal was to measure the fraction of energy transported away from the turbulent mixed layer as internal waves.

A. Experimental set-up

The experiments were conducted in a transparent acrylic tank of length 47.6 cm, width 9.7 cm, height 50.0 cm, and wall thickness of 0.8 cm. An initially linear stratification was created using the classic double-bucket apparatus[20] and the resulting density profile was measured using a vertically traversing conductivity probe (MSCTI, Precision Measurement Engineering). In most experiments, the buoyancy frequency ranged between $N = 1.38\,\mathrm{s}^{-1}$ and $1.50\,\mathrm{s}^{-1}$.

After filling the tank a ridged conveyor belt spanning the width of the tank was partially submerged with the lower part of the belt situated approximately 1 cm below the surface in the tank. The ridges, which spanned the belt-width, had height 0.4 cm, thickness 0.1 cm, and were spaced apart by 2 cm. These acted to increase the effective stress of the moving belt upon the fluid. Two driving wheels on either end of the tank were connected via gears to synchronize servo motors that moved the belt at linear speeds between $U = 4$ and 20 cm/s. The belt speed was held constant for any particular experimental run.

For the sake of efficiency, several runs were often performed with the same experimental setup. In a typical sequence, a run would be performed with the belt moving at relatively slow speed for approximately 10 min. The system would then be allowed to come to rest over at least 20 min. Then, at the start of the next run, the belt would then be set to move again at a higher, but constant speed. This sequence was repeated up to four times. After an initial transient phase in which the conveyor belt first applied stress to the surface mixed-region established from previous runs, a quasi-steady recirculating turbulent flow was established in the mixed region. Test experiments in which the belt initially moved quickly over a uniformly stratified ambient confirmed that the statistical properties of the turbulence and waves were insensitive to the initial conditions.

In some experiments the near surface fluid was dyed with food colouring and the belt was set to move at constant speed for many hours in order to examine the deepening of the surface mixed layer. In most other experiments the near surface was seeded with particles so that mean and fluctuation velocities could be measured using particle image velocimetry (PIV). The characteristics of the generated internal waves were measured in the underlying stratified fluid using synthetic schlieren.[21]

Figure 1 shows schematic representations of density profiles before and after an experiment and it shows a composite image in which particles are illuminated in the mixing region for PIV analysis and internal waves are visualized in the underlying fluid using synthetic schlieren. The tank as a whole is shown in Figure 1(a)). The inset snapshot extending between $z = 0$ and -10 cm shows the window used by PIV to measure the turbulent eddy field in the surface mixed region. Below this the inset grayscale image shows the vertical displacement field resulting from internal waves in the underlying stratified fluid as computed using synthetic schlieren. Details of the PIV and schlieren methods are presented in Secs. II C and II D below.

The lighting conditions required for PIV and for synthetic schlieren were in conflict. The use of PIV required the lab lights to be turned off while synthetic schlieren needed bright back lighting. Although technically possible for these two techniques to be done concurrently,[22] this was not done for our experiments. For early experiments, an experimental sequence was configured for either PIV or synthetic schlieren. Data gathered for each method were compared between experiments with the same conveyor belt speed, stratification, and mixed-layer depth. For later experiments, two cameras were set up so that the imaging modality between PIV and synthetic schlieren could be switched quickly between essentially the same experiment. We assume that we can compare the energy densities of the turbulence and the waves as if both were measured from the same experiment.

B. Deepening of the mixed layer

Numerous experiments have been carried out to examine the deepening of a statistically stationary or sheared turbulent mixed layer overlying either a fluid of moderately larger, but uniform,

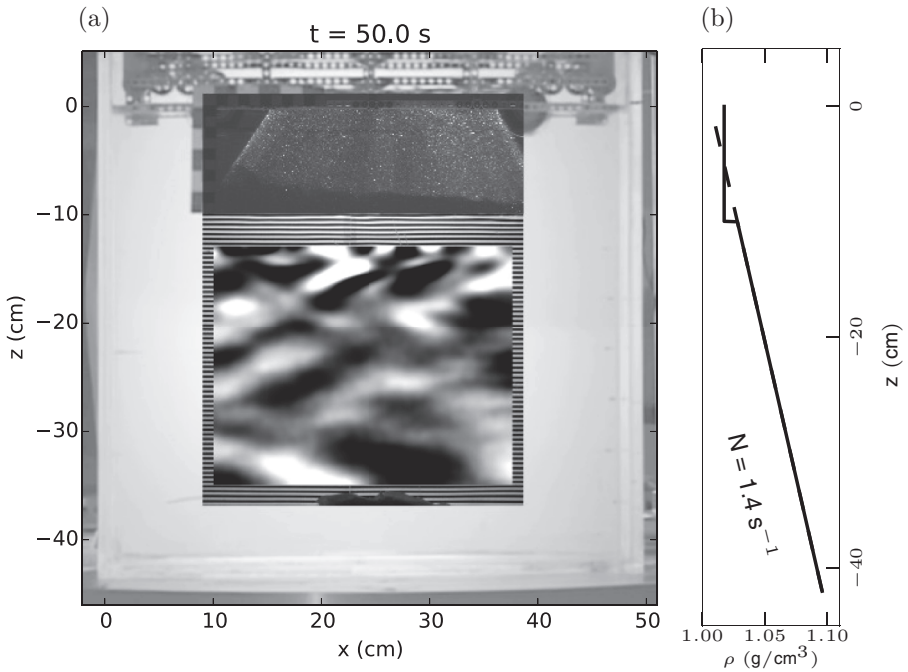

FIG. 1. (a) Composite image of turbulence- and wave-visualization methods used in laboratory experiments. PIV records particle motion in the mixed region below the surface (at $z = 0$). Synthetic schlieren measures the apparent distortion of a screen of black and white lines behind the tank (between $z = -14$ and -36 cm) and from this computes the corresponding vertical displacement of the fluid by waves. (b) Initial density profile (dashed line which extends linearly to the bottom of the tank) and a characteristic density profile during an experiment showing near uniform density in the surface mixed region with uniform stratification beneath (solid line).

density or a uniformly stratified fluid.[7,19,23–29] Particularly in the case of an underlying uniformly stratified layer, the depth of the mixed layer with time, $D(t)$, is expected to have a relatively small power law exponent in part because of the decay of turbulent kinetic energy with distance from the source and also because the density jump across the interface becomes larger as the interface deepens. Ignoring the former effect, the interface depth is predicted to increase with time[7,19] as $D \propto t^{1/3}$. This was confirmed by experiments of surface shear overlying an annular tank filled initially with uniformly stratified fluid.[19] The combination of unidirectional shear and the relatively short time over which the deepening was measured (of the order of a few minutes), dictated that there was little energy dissipation between the surface and interface. Accounting for the kinetic energy decay with depth in an oscillating grid-generated turbulence experiment, Linden[7] predicted $D \propto t^{2/15}$ at late times. This behaviour was consistent with laboratory experiments of Linden[7] and E and Hopfinger,[25] the latter of whom proposed $D \propto t^{1/8}$.

Though not the focus of this work, we performed some experiments in which the conveyor belt ran continuously for several hours and we measured the mean depth of the interface between the turbulent mixed region and the underlying stratified fluid as it descended over time. The vertical time series in Figure 2(a) shows the position of the interface with respect to the surface at $z = 0$ as it evolves in time after the belt begins to move at $t = 0$. In the first minute, the interface rapidly descends of the order of 10 cm. After that time, the descent is much more gradual taking hours to descend another 20 cm. After converting the time series to a bi-level image, a contour was fit to the interface between the dyed turbulent mixed region and the clear underlying stratified fluid. From this we determined the depth, D, of the mixed layer as it increased with time. This was measured in three experiments, one with $U = 8$ and $N = 1.4\,\mathrm{s}^{-1}$ and the other two with $U = 16$ cm/s and $N = 1.8$ and $1.9\,\mathrm{s}^{-1}$.

Figure 2(b) shows log-log plots of the nondimensional depth, ND/U versus nondimensional time Nt computed for the three experiments. These suggest that $D(t)$ satisfies a power law relationship,

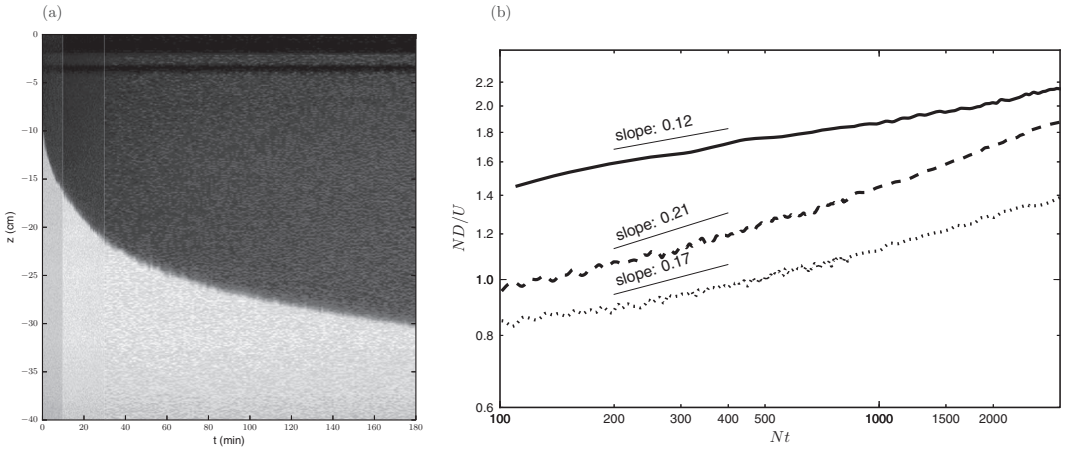

FIG. 2. (a) Vertical time series showing the deepening of the mixed layer (dark fluid) in an experiment with $U = 8$ cm/s and (b) log-log plots of nondimensional mixed-layer depth vs nondimensional time determined from experiments with $U = 8$ cm/s, $N = 1.4\,\mathrm{s}^{-1}$ (thick solid line), and $U = 16$ cm/s, $N = 1.8\,\mathrm{s}^{-1}$ (dashed line), and and $U = 16$ cm/s, $N = 1.9\,\mathrm{s}^{-1}$ (dotted line). Vertically offset best-fit lines are shown above each curve with slope indicated.

although the exponent varies somewhat between experiments. In the experiment with slow belt speed we found $ND/U = 1.4\,(Nt)^{0.12}$, whose exponent is consistent with the prediction of Linden[7] for grid-generated turbulence overlying a stratified layer. However, in the experiments with the fast belt speeds we found $ND/U = 1.0\,(Nt)^{0.21}$ for $N = 1.8\,\mathrm{s}^{-1}$ and $ND/U = 0.82\,(Nt)^{0.17}$ for $N = 1.9\,\mathrm{s}^{-1}$. In these two experiments we found that the rightward-moving flow just underneath the belt plunged downward significantly at the right-side of the tank before flowing leftward as an undercurrent at the base of the mixed region. Entrainment into this plunging flow changed in time as the mixed-layer deepened and the plunging extended less below the base of the mixed region.

All of this is to say that the dynamics of entrainment in our experiments is more complex than that of statistically steady turbulence. Because the plunging we observed was an artifact of the experiment set-up with no counterpart in nature, we did not explore this dynamics in greater detail. Instead we focused upon internal wave generation by sheared turbulence at the base of the mixed region.

C. Turbulence measurements

After rapid deepening in the first minute, the mixed region evolved slowly compared to the time scales associated with turbulence in the mixed layer and waves in the underlying stratified layer. Hence, in the study of the properties and energetics of the turbulence and waves we assume that the depth of the mixed layer is constant over the few minutes in which statistics are gathered, with data collection beginning a few minutes after the start of an experiment.

The turbulence length and time scales were measured using PIV. Nearly neutrally buoyant, salt-water saturated Pliolite particles were injected into the mixed layer about 2 cm below the surface. The particles tracked the motions of the fluid and also marked the depth of the mixed region. The laser light sheet was created by passing a 600 nm, <1 mW beam through a non-Gaussian lens (45° SNF Straight Line, Lasiris, Inc.). This illuminated a plane of the particles, the upper mixed layer of the tank, whose motion was then captured by a JAI digital camera with a resolution of 1372 × 1024 recording at 24 frames/s. Figure 3 shows an example of an image obtained, a close-up of the inset image in Figure 1(a).

We processed the images of the illuminated particles using an open source, two-pass, cross-correlation PIV software[30] called CIVx. The first cross-correlation estimated the velocity field and the second used this as an estimate to make a more accurate analysis of the velocity field in a second pass. We chose an interrogation window size of 32 × 32 pixels and search window size of 64 × 64 pixels giving a 100% overlap between adjacent grid boxes. The output of CIVx was a velocity

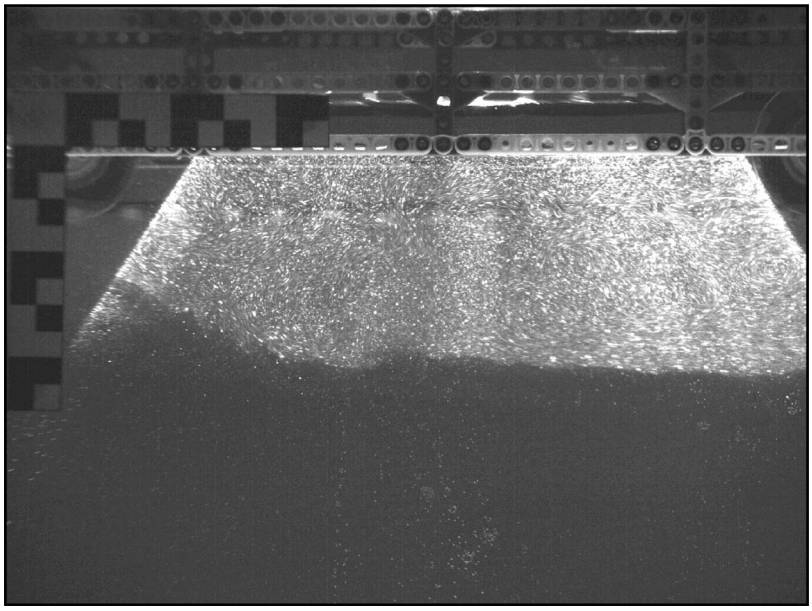

FIG. 3. Close-up of mixed region in Figure 1(a) showing particles in an approximately 8 cm deep mixed layer illuminated by a laser light sheet recorded during a PIV experiment.

field $\vec{u} = (u, w)$ with horizontal and vertical components on a two dimensional grid at each time. We only considered a region of interest in the mixed region below the conveyor belt, away from the side walls, and above the stratified region.

An example of the instantaneous velocity field measure by PIV is shown in Figure 4(a). Further processing was required to extract the velocity field associated with turbulent eddies and hence find the turbulent kinetic energy density. The velocity field was averaged in time over 100 s beginning 3 min after the start of an experiment to give the mean recirculating flow in the mixed layer, $\langle\vec{u}\rangle$, as shown in Figure 4(b). Because the conveyor belt moved from left to right along the top of the tank the mean circulation was clockwise in the mixed layer with a strong near-surface flow and (not in the field of view of the light sheet) a plunging downward flow on the right-hand side of the tank. Throughout the bulk of the mixed region was a broad upwelling region with moderate leftward component of velocity near the bottom of the mixed region.

Given the instantaneous and mean velocity fields, we computed the fluctuation velocity as the difference between the two: $\vec{u}' = \vec{u} - \langle\vec{u}\rangle$. This is shown in Figure 4(c). The scale of the fluctuations, of the order of 1 cm/s, was comparable to the scale of the mean circulation and coherent structures in the fluctuation velocity field were manifest on length scales comparable to the tank width.

As a consequence of the spanwise uniform forcing as well as the tank's aspect ratio in the horizontal, the energy-containing eddies in the turbulent flow were observed to be quasi-two-dimensional. For this reason, we neglected the spanwise component of the velocity (v') in the definition of the average turbulent kinetic energy density within the mixed region:

$$E_{\mathrm{TKE}} = \frac{1}{A}\int\int \frac{1}{2}\rho_0\left(u'^2 + w'^2\right) dA, \tag{1}$$

in which A is the area over which fluctuation velocities were measured.

Figure 4(d) shows the evolution of the turbulent kinetic energy over time beginning 3 min after the start of an experiment. In this example, as in all other experiments performed, there was no observed trend showing either increasing or decreasing E_{TKE} over the several minute duration of each experiment. We computed the time average of the E_{TKE} to get an estimate of the turbulent energy density for each experiment as a function of conveyor belt speed.

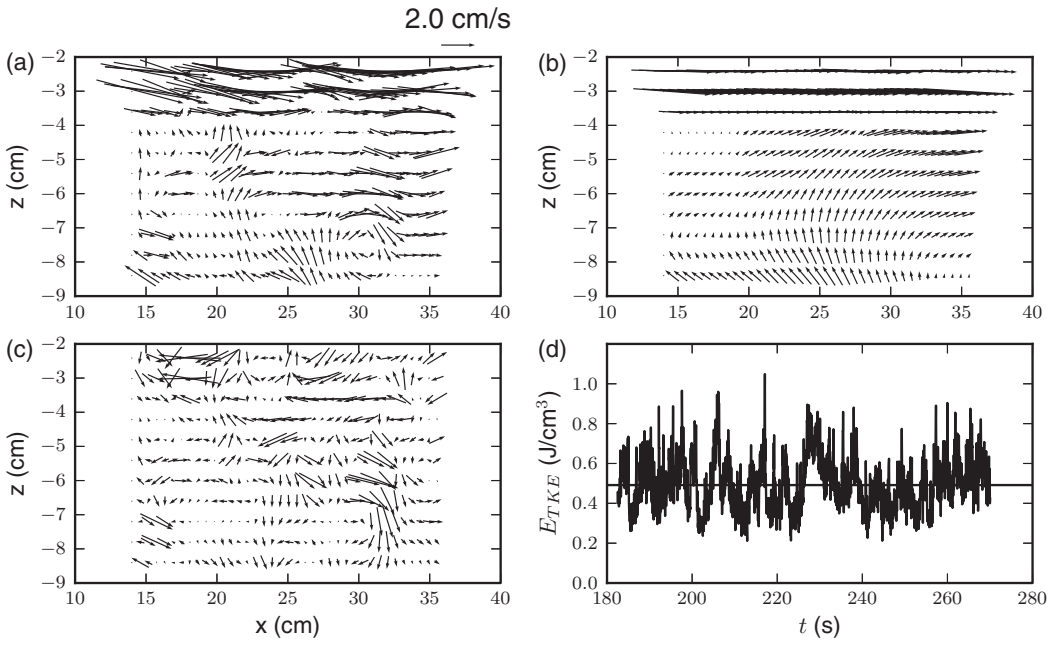

FIG. 4. For an experiment with $U = 12$ cm/s and $N = 1.47\,\mathrm{s}^{-1}$, (a) instantaneous velocity in mixed layer determined by PIV, (b) time-averaged velocity, (c) fluctuation velocity (instantaneous minus averaged), and (d) turbulent kinetic energy density of the mixed layer versus time (thick line) with the time-average indicated by the dashed line.

D. Wave measurements

Synthetic schlieren[21] was used to provide quantitative measurements of the internal waves generated in the lower stratified region. Behind the tank fluorescent lights illuminated a screen of horizontal black and white lines. The lines were 0.2 cm thick and the screen was placed 10 cm behind the tank. A digital video camera recorded the image of the screen through the salt-stratified fluid.

Internal waves alternately stretch apart and compress together isopycnal surfaces, locally changing the density gradient and, hence, the local value of the squared buoyancy frequency. Because the index of a refraction varies with salinity, these changing density gradients resulted in apparent distortions of the image of lines on the screen. Assuming the waves are approximately spanwise-uniform (a reasonable assumption for waves having wavelength longer than the tank width), the change in N^2 due to waves can be measured directly from the measured apparent vertical displacement of lines in the image. For our purposes, it was practical to measure the time rate of change of the squared buoyancy frequency due to waves, $\Delta N^2{}_t$, because this field is proportional to the vertical displacement field and because the time derivative acts to filter out long time-scale disturbances. An example of the computed vertical displacement field superimposed on the image screen below the mixed region is shown in the center of the composite image of the tank in Figure 1(a).

Movies of the $\Delta N^2{}_t$ field showed wavepackets propagating predominately downwards from the mixed region, as clearly evident from observations of the phase velocity having an upward vertical component. Although the experiments were run for sufficiently long time that the waves were expected to reflect off the tank bottom and propagate back upward into the field of view, the reflected signal was not strong. With typical wavenumber magnitudes of $k \sim 0.5\,\mathrm{cm}^{-1}$, the timescale for viscous attenuation of the waves was $(k^2\nu)^{-1} \sim 400$ s, significantly longer than the typical time of $\sim$30 s for waves to traverse the depth of the tank at the vertical group speed. With typical frequencies of $\omega \sim 1\,\mathrm{s}^{-1}$, the Reynolds number associated with the waves was $\mathrm{Re} = 400$, large enough that viscous effects should not play a significant role during the analysis of the waves over a 2 min time period. With these considerations, we believe a bottom-reflected wave signal was not strong primarily as a result of dispersion of wavepackets launched from the base of the mixed region.

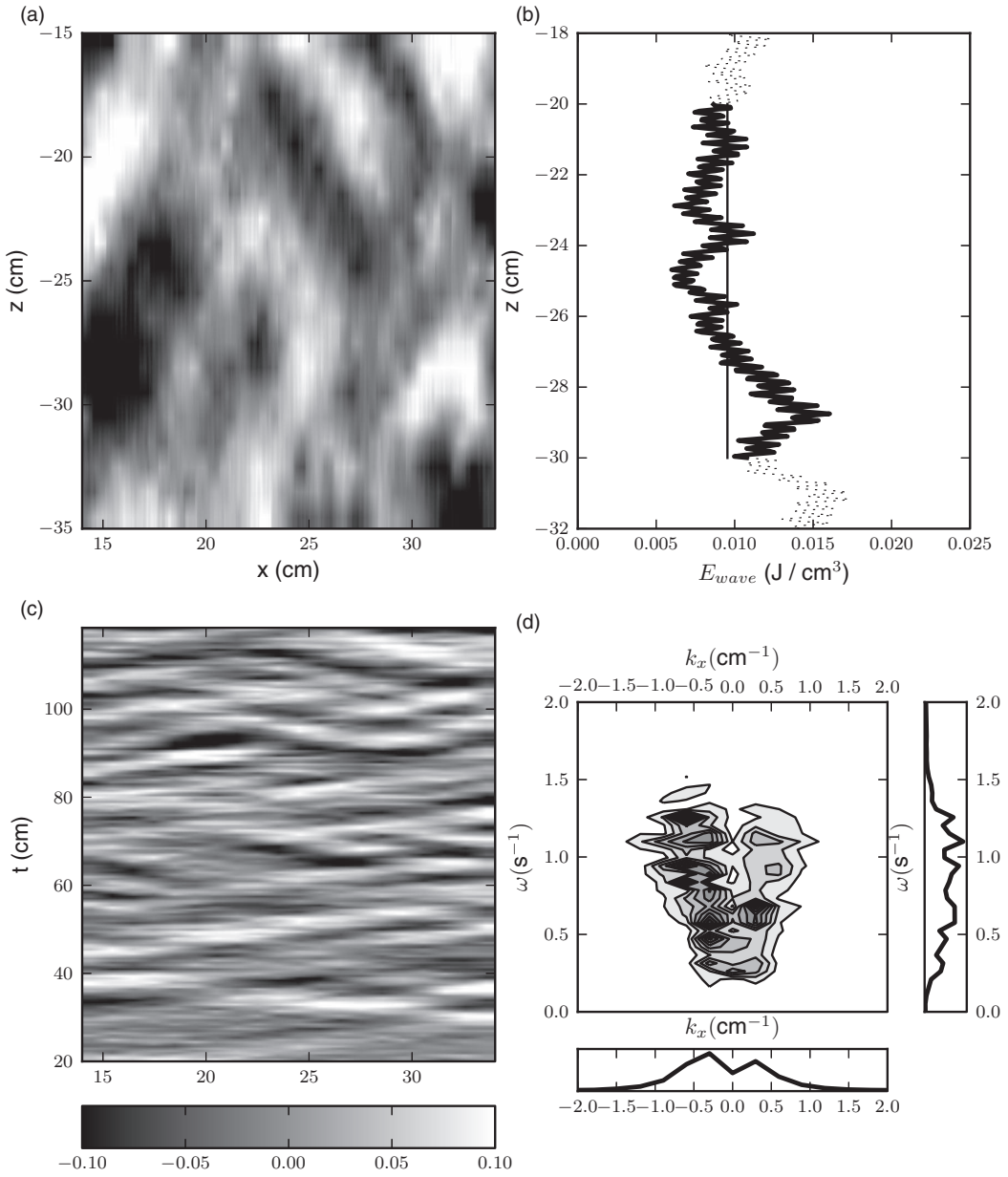

FIG. 5. Wave analyses for experiment with $U = 12$ cm/s, $N = 1.4\,\mathrm{s}^{-1}$ showing (a) snapshot of the $\Delta N^2{}_t$ field at $t = 50$ s; (b) wave energy density as a function of depth (thick curve) with average value between $z = -20$ and -30 cm indicated by vertical dashed line; (c) horizontal time series of this field at $z = -25$ cm; and (d) $\Delta N^2{}_t$ spectrum computed from horizontal time series at times between $t = 30$ and 120 s.

A snapshot of the internal wave vertical displacement field is shown in Figure 5(a). Extracting a horizontal slice through a sequence of these snapshots in time, we constructed horizontal time series of waves passing a fixed vertical level, as shown in Figure 5(b). The slope of the tilting lines of constant phase gives a measure of the horizontal phase speed. (Explicitly the slope is ω/k_x, which differs from the horizontal component of the phase velocity c_{px}.) In the time series shown in Figure 5(b), the slopes are both positive and negative, indicative of internal waves with rightward and leftward horizontal phase speed.

Spectra of the horizontal time series were used to quantify the phase speed information and to extract information about the characteristic scales and energy associated with the waves. For

example, the grayscale contours in Figure 5(c) show the spectrum computed from the horizontal time series in Figure 5(b). The somewhat stronger signal on the up and leftward branch of this spectrum indicates that more power is associated with leftward-propagating waves. This result is consistent with the mean circulation near the base of the mixed region being leftward.

To the right and below the contour plot in Figure 5(c) are individual plots of the frequency and horizontal wavenumber spectrum. Whereas other experiments of internal waves generated by turbulence[4,5,8] have exhibited a strong peak in the wavenumber-frequency spectrum, here we find that the frequency spectrum exhibits significant power between the buoyancy frequency cut-off of $N = 1.4\,\mathrm{s}^{-1}$ and $0.2\,\mathrm{s}^{-1}$. Consistent with those other experiments, however, the peak of the spectrum occurs for waves with frequency about $\omega^\star = 1.0 \pm 0.1\,\mathrm{s}^{-1}$, corresponding to waves propagating at an angle $\Theta^\star = \cos^{-1}(\omega^\star/N) \simeq 45^\circ$.

To compute the wave energy, the spectra of ΔN_t^2 in horizontal wavenumber (k_x) and frequency (ω) space were low-pass filtered. We restricted $\omega < N$ to consider only freely propagating internal waves, and we restricted $|k_x| \leq 1.0$ to eliminate high spatial frequency noise. Given $A_{\Delta N_t^2}(k_x, \omega)$ and assuming the waves are sufficiently small amplitude that linear theory applies, the polarization relations for internal waves[31] were used to compute the amplitude of the the vertical displacement field, ξ, in Fourier space through

$$A_\xi = A_{\Delta N_t^2}/(N^3 k_x \sin\Theta), \tag{2}$$

in which $\Theta = \cos^{-1}(\omega/N)$. Typical vertical displacement amplitudes are found to be of the order $||A_\xi|| \simeq 0.05 k_x^{-1}$, sufficiently small that the linear theory approximation is justified. Given that the energy density associated with an internal wave with horizontal wavenumber k_x and frequency ω is

$$E(k_x, \omega) = \frac{1}{2}\rho_0 A_\xi^2 N^2, \tag{3}$$

the results across the filtered spectrum were integrated to give the total wave energy density:

$$E_{\mathrm{wave}} = \int\int E(k_x, \omega)\, dk_x\, d\omega. \tag{4}$$

Repeating this procedure for a horizontal time series taken at different vertical levels allowed us to plot E_{wave} as a function of depth, z, as shown, for example, in Figure 5(d). Here the wave energy density was approximately constant below $z = -20$ cm. A vertical average for z between -30 cm and -20 cm was taken to obtain a value for the average wave energy density below the mixed region. This we could compare with the turbulent kinetic energy density in the mixed region, E_{TKE}, for experiments performed with a range of conveyor speeds, U.

E. Experiment results and discussion

Generally, we found that the turbulent energy density increased with belt speed U and decreased with mixed-layer depth D. Although it is difficult to see considering the scatter within the data, the energy appears to scale quadratically with U/ND as would be expected from dimensional analysis. This quadratic relationship is much more apparent when groups of experiments starting from the same initial stratification are considered separately.

A summary of the results of the energy analyses applied to the turbulence and internal waves is presented in Figure 6. Here E_{TKE} and E_{wave} determined for each experiment are plotted versus the square of non-dimensional conveyor belt speed $\hat{U} = U/ND$. Notwithstanding the significant scatter, there is an overall pattern in the results. Both turbulent and wave energy density appear to scale quadratically with $\hat{U}$. Using a least-squares linear fit forced to pass through the origin we found $E_{\mathrm{TKE}} = 1.44\hat{U}^2$ J/cm^3 and $E_{\mathrm{wave}} = 0.031\hat{U}^2$ J/cm^3. The wave energy density was approximately a constant fraction of the turbulent energy density since the ratio $E_{\mathrm{wave}}/E_{\mathrm{TKE}}$ of the slope of the best-fit lines is 2.1%

As an alternate approach, we compared the wave and turbulent energy densities pair wise for experiments where PIV and synthetic schlieren measurement were made for the same experiment as

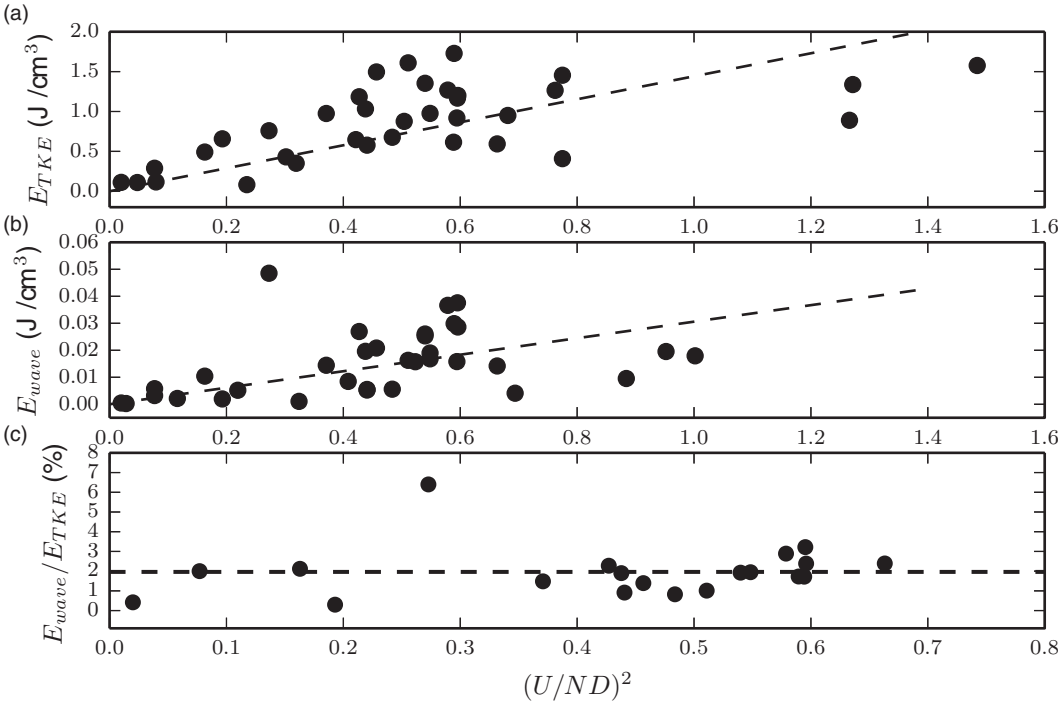

FIG. 6. Comparison between energy density of the mixed layer and stratified layer. (a) Turbulent kinetic energy density and (b) wave energy density as a function of non-dimensional conveyor belt speed. A best-fit linear trend is shown with a dashed line for each plot. (c) For a subset of the experiments, the ratio of wave energy density to turbulent kinetic energy density is calculated directly. The ratio of turbulent kinetic energy density to wave energy density is about 2%.

shown in Figure 6(c). It this case, the ratio of wave energy density was independent of U/ND with an average value of $E_{\text{wave}}/E_{\text{TKE}} = 2.0\%$.

There was a significant amount of temporal variability in the turbulent kinetic energy measurements (e.g., Figure 4(d)). If the experiments were run for a longer duration, this may have improved the estimate of the average turbulent energy measurements and thus reduced the amount of scatter in Figure 6(a). The anomalously large value of wave energy in Figures 6(b) and 6(c) at $(U/ND)^2 = 0.27$ is likely due to the field of view chosen for synthetic schlieren including part of the strongly stratified pycnocline just below the mixed layer. That would have led to an overestimate of the wave energy for that particular experiment.

We conclude that, to an order of magnitude, internal wave energy density is about 2% of turbulent kinetic energy density.

III. NUMERICAL MODEL

We performed numerical simulations in order to gain additional insight into the generation of internal waves by eddies in a shear flow. The model configuration was not designed to replicate the laboratory experiments. On the contrary, it was set up in a two-dimensional domain with no end walls. As we will show, the simulations nonetheless capture the qualitative results of the experiments.

A. Model set-up

We used the numerical model *Diablo* to simulate the evolution of an unstable shear flow overlying a uniformly stratified fluid.[32] This model had been used previously to simulate a turbulent boundary Ekman layer in a stratified fluid that launched upward-propagating internal waves.[15]

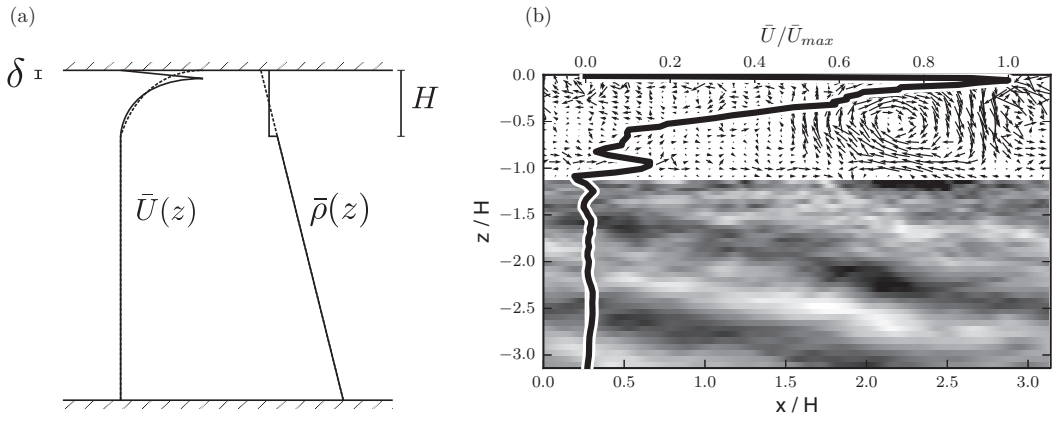

FIG. 7. (a) Typical background density profile, $\bar{\rho}(z)$, prescribed at the start of a simulation. (b) An example of the output of a simulation run with $P_{x0} = 4$ shown at time $Nt = 9$. The upper region shows the perturbation velocity field of the mixed layer. The lower region shows the vertical displacement field. The solid line is the mean horizontal velocity. (Multimedia view) [URL: http://dx.doi.org/10.1063/1.4895645.1].

The horizontally spectral and vertically finite-difference code solved the Navier-Stokes equations in the Boussinesq approximation. For our simulations, we configured the model domain to have horizontal periodic boundary conditions and with no-slip top and bottom boundary conditions. The numerical domain was set to be so deep that internal waves would not propagate from the base of the turbulent region to the bottom of the domain over the duration of the simulation.

The background density, $\bar{\rho}$, was initialized as a mixed layer of depth H overlying a linearly stratified ambient, as illustrated in Figure 7(a). Explicitly, we set

$$\bar{\rho}(z) = \begin{cases} \rho_T, & 0 \geq z \geq -H \\ \rho_T + \Delta\rho + \Gamma(z+H), & z < -H \end{cases}, \tag{5}$$

in which ρ_T is the density in the surface mixed-layer of thickness H, $\Delta\rho$ is the density jump between the mixed-layer and the underlying uniformly stratified fluid, and the constant density gradient in the stratified fluid is denoted by Γ. The length and time scales of the simulation were implicitly set by choosing $H = 1$ and by choosing Γ so that $N^2 = -g\Gamma/\rho_T = 1$. In control runs we set $\rho_T = \Delta\rho = 0.5$.

The velocity field was initialized to be at rest except within the model mixed-layer where Gaussian noise was added and filtered to ensure that it was divergence-free. A shear flow was generated in the mixed region through application of a horizontal pressure gradient within a thin layer of depth δ along the top of the domain:

$$\frac{dp}{dx}(z) = \begin{cases} -P_{x0}, & 0 > z \geq -\delta \\ 0, & z < -\delta \end{cases}, \tag{6}$$

in which the negative in front of the forcing parameter P_{x0} emphasizes that the pressure gradient forces a rightward flow. The forcing was continuous starting at time $t = 0$. The strength set by the constant value of P_{x0}, which ranged between 1 and 6 in non-dimensional units. In all runs we set $\delta = 0.1H$. Together with the no-slip top boundary condition, the forcing had the effect of creating a shear flow with an inflection point at the surface that rendered it unstable. An example of the resulting horizontally averaged flow in the model mixed-layer is shown by the solid line in Figure 7(a).

The domain size, expressed in terms of the mixed-layer depth, was $L_x = 3.14H$ in the horizontal and $L_z = 40H$ in the vertical. It was assumed that the length scales of the turbulence were shorter than that of the waves and thus required higher resolutions. Hence the numerical grid was stretched

in the vertical to allow more points in the mixed-layer region and less in the stratified region. A stretching function was used in the vertical so that grid points were situated at

$$z[j] = L_z \left(\frac{\tanh(Sj/n_z)}{\tanh(S)} - 1 \right) \tag{7}$$

for $j = 0 \ldots n_z$. Here S is the grid stretching parameter. In the limit as S goes to 0, the vertical spacing of grid points becomes uniform. We used a value of $S = 2.0$. With $n_z = 256$, this corresponded to the vertical spacing between grid points increasing from $\Delta z = 0.023$ at the top of the domain to $\Delta z = 0.324$ at the bottom.

The code was run with spatial resolution $n_x = 256$ in the horizontal and $n_z = 256$ in the vertical. We found that doubling both the vertical and horizontal resolutions did not significantly change the results. The fields were advanced in time with a fixed step of $\Delta t = 0.0001$. With these values, they took approximately 4 h to complete a run on a single processor.

An example of the model output is shown in Figure 7(b) (Multimedia view). The solid black is the horizontally averaged velocity profile. Motion in the upper mixed layer is visualized with arrows indicating the velocity field. In the lower stratified layer, the grayscale indicates values of the vertical displacement field. This snapshot is shown at a time when a strong coherent vortex and underlying waves are clearly visible.

B. Analysis method

The energetics of the simulated two-dimensional turbulence and underlying internal waves were analyzed similar to the methods used to analyze the laboratory experiments. However, for the simulations the mean horizontal flow, $\bar{U}(z, t)$, was determined by horizontal averaging rather than temporal averaging. As in the experiments, the fluctuation velocity was defined by $(u', w') \equiv (u - \bar{U}, w)$ and, similar to (1), the turbulent kinetic energy density was calculated by

$$E_{\mathrm{TKE}} = \int_{-H+0.1}^{-\delta-0.1} \int_0^{L_x} \frac{1}{L_x(H - 0.2)} \frac{1}{2} \rho_0 (u^2 + w^2) dx dz. \tag{8}$$

The vertical bounds of the integral were set to measure the turbulence within the mixed layer away from both the interface and the upper frictional layer. The energy density was computed for a range of time $5 < Nt < 20$ and then averaged to get a representative value for E_{TKE}. E_{TKE} had no mean trend over time.

To measure the energy of the waves, the vertical displacement field, ξ, was determined from the density field, ρ, within the stratified region through the relation

$$\xi(x, z, t) = \frac{1}{\Gamma} \left(\rho - \frac{d\bar{\rho}}{dz} \right). \tag{9}$$

From a horizontal time series of ξ at a fixed vertical position, the wave energy density was computed using the method employed in the laboratory experiments: Fourier transforming, filtering and integrating over all frequencies and wavenumbers. The process was repeated for horizontal time series taken from a range of vertical positions, $-9H \leq z \leq -2H$. The average of these results was taken to give a representative value for the energy density of the wave field below the upper mixed layer.

C. Simulation results

Movies of the evolution of the wave field and the turbulent field show that downward propagating wavepackets were launched when sufficiently large eddies, on the scale of the mixed layer depth, interacted with the interface. If an eddy was relatively stationary when impacting the interface, then wavepackets were observed to have both leftward and rightward horizontal phase velocities. If an eddy interacted with the interface while being carried rightward (in the direction of the mean flow), the horizontal phase velocity of the generated waves was rightward alone with magnitude close to the speed of the eddy. In the former case, the waves were generated in a manner similar to an

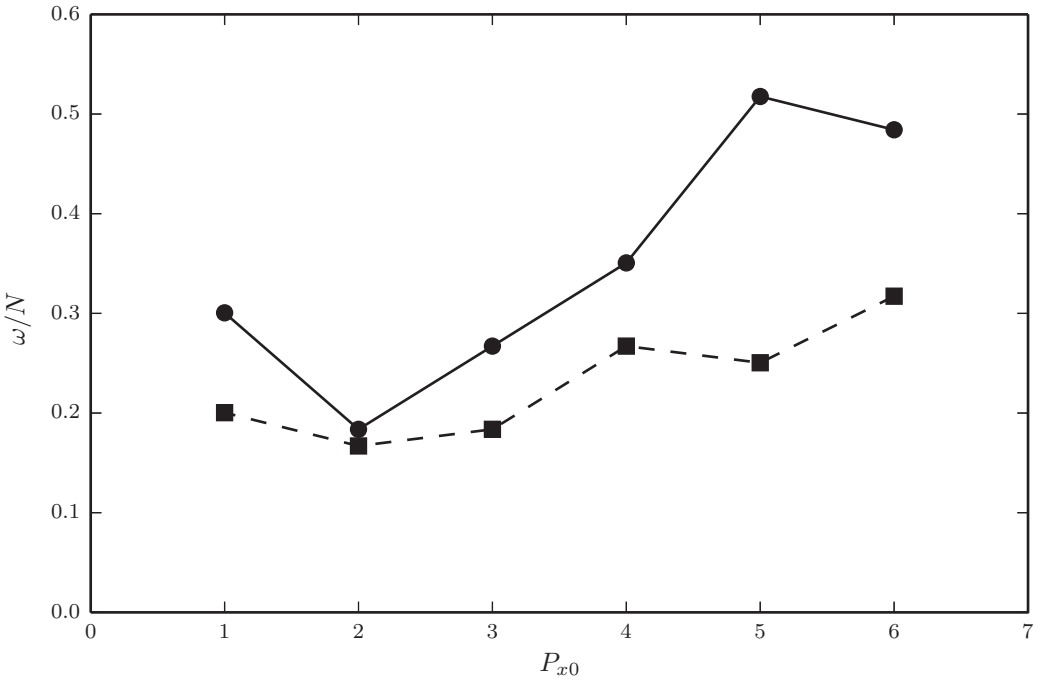

FIG. 8. Dominant relative frequency ω/N of the internal waves based on the spectrum of the horizontal time series at $z = -6H$ plotted for simulations with different values of surface forcing P_{x0}. The solid and dashed lines connect data determined from simulations with $L_x = 3.14H$ and $L_x = 1.57H$, respectively.

oscillating cylinder in which the time scale for the eddy impinging into the stratified layer set the time scale of the waves. In the latter case, the waves were generated in a manner similar to flow over topography, in which the speed and horizontal scale of the translating eddy set the time scale of the waves. However, unlike the generation by oscillating and translating bodies, here the eddy can be influenced by the process of wave generation—itself deforming or changing its translational speed as a result of losing momentum and energy to waves.

The dependence of the time scale of the waves upon the forcing is shown in Figure 8, which plots the dominant wave frequency as a function of P_{x0}. As P_{x0} increases, the frequency of the waves increases. Halving the horizontal extent of the domain decreased the frequency of the waves. With $L_x = 3.14H$, the observed horizontal extent of the largest eddies was close to the horizontal extent of the domain. Correspondingly we found internal waves had peak horizontal wavenumbers of $k_xH = -2 \pm 2$, for all values of $|P_{x0}|$. In simulations with $L_x = 6.28H$ and $12.56H$ the peak horizontal wavenumbers were found to be $k_xH = -2.0 \pm 0.5$ and -1.5 ± 0.5, respectively, with $P_{x0} = 4$. As expected by viewing movies of the simulations (as in Fig. 7(b) (Multimedia view)), the horizontal scale of the waves was set by the size of the largest eddies, which in turn is set by the mixed-layer depth.

In Figure 9 the energy densities of turbulence in the model mixed-layer and of waves in the stratified layer are plotted against the forcing parameter P_{x0}. The ratio of these two energies (Figure 9(c)) shows a moderate increase with increasing P_{x0} but, on average, is 3%.

Changes to the horizontal domain size had no significant effect on the energy density. When the density ρ_T was doubled while keeping the density jump and density gradient the same, the energy of both the turbulence and waves did not substantially change. However, doubling the thickness of the mixed layer increased the size of the eddies. The energy ratio between the waves and the turbulence decreased by increasing the size of the mixed layer. Doubling the density jump also decreased the energy ratio but to a lesser extent than doubling the mixed layer thickness. The turbulent energy density exhibited no dependence on the thickness of the mixed layer or on the density jump.

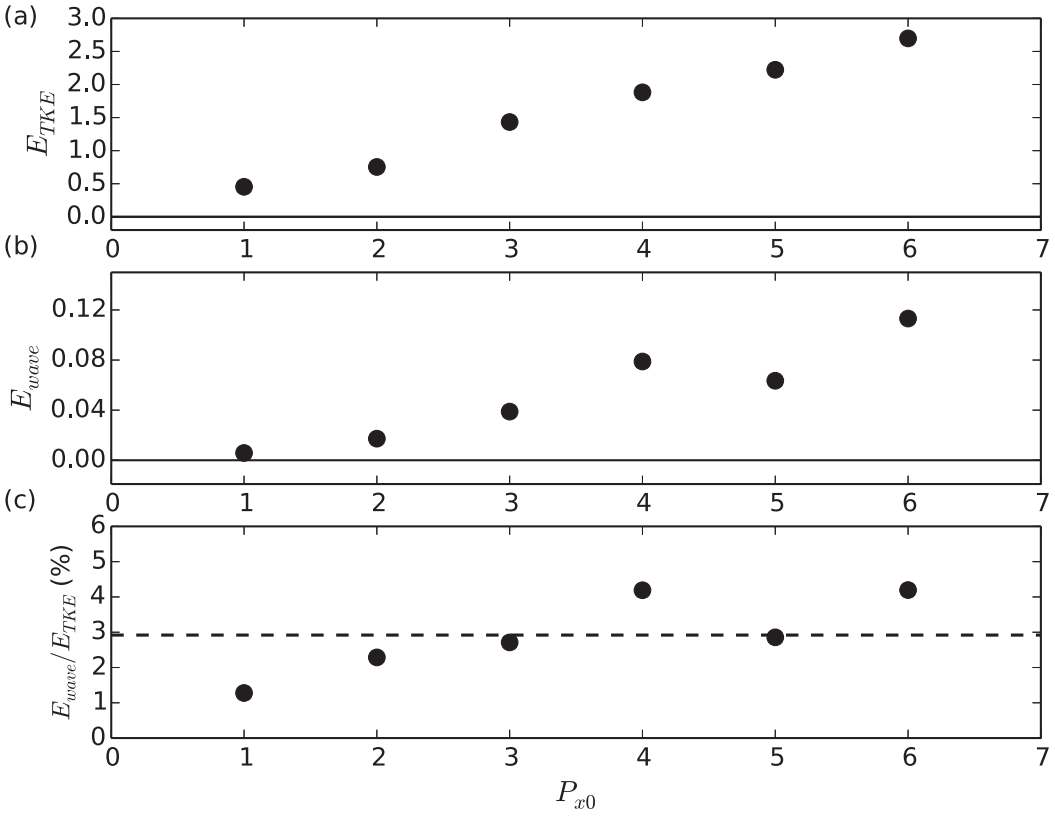

FIG. 9. Summary of energy measurements over several simulations. (a) Energy density of the turbulence plotted against the magnitude of the pressure gradient, P_{x0}. (b) Energy density of the waves. (c) Ratio $E_{\text{wave}}/E_{\text{TKE}}$ plotted against P_{x0}. The dashed horizontal line shows the average.

IV. DISCUSSION AND CONCLUSION

Experiments and simulations of internal waves generated by turbulent shear flows show that internal waves extracted between 1% and 3% of the turbulent kinetic energy density in the upper mixed layer. By this measure, the simulations well-captured the partition of energy even though they were only run in two dimensions. This suggests that wave generation by eddies in shear was dominated by two-dimensional processes in the laboratory experiments. We are confident that the experiments captured the dynamics of wave generation by spanwise coherent vortices aligned with the vorticity of the mean shear. In particular, the presence of the tank walls in the laboratory setup was not critical to the wave generation process, for example, through the plunging flow on the right-hand side: we did not observe significant wave generation from that side of the tank and the numerical simulations well-captured the wave generation mechanism in a horizontally periodic domain.

The numerical models need to be extended to three dimensions to examine what effects 3D turbulent structures and a broad frequency spectrum forcing have on the wave field and whether this produces waves of the characteristic frequency that are typically associated with turbulently generated waves.

Results from the numerical model suggest that the primary mechanism for internal wave generation is spanwise-coherent turbulent eddies in shear that are carried over the density interface. This is not a generation mechanism currently parametrized in ocean models. Although as a fraction, 1%–3% energy extraction may appear small, the total amount of turbulent kinetic energy in the upper mixed layer of the ocean is very large. From observations, it has been estimated that approximately 20 TW of wind power is imparted by surface wind stresses to the upper ocean.[33]

The vast majority of this energy (∼19 TW) is estimated to go into surface waves and turbulence and only 0.6 TW into internal waves near the inertial frequency. Our laboratory and numerical experiments suggest that of the order of 1% of energy input by surface stresses on a turbulent mixed layer above a stratified ambient fluid is radiated away by non-hydrostatic internal waves. This implies that of the order of 0.2 TW is transferred to the internal wave field. Since these are high frequency waves, it is expected that most of this wave energy will remain around the depths spanned by the thermocline. Even though this is only an order of magnitude estimate, it still suggests that the generation of internal waves by turbulence is an important mechanism for energy transport and consequent mixing in the upper ocean below the surface mixed layer. When analyzing the energy pathways in the ocean, especially for the meridional overturning circulation, the uncertainties are often described in units of the order of 0.1 TW and so this generation mechanism should be included.

[1] L. H. Kantha and C. A. Clayson, "On leakage of energy from turbulence to internal waves in the oceanic mixed layer," Ocean Dyn. **57**, 151–156 (2007).
[2] P. Bonneton, J.-M. Chomaz, and E. J. Hopfinger, "Internal waves produced by the turbulent wake of a sphere moving horizontally in a stratified fluid," J. Fluid Mech. **254**, 23–40 (1993).
[3] A. M. Abdilghanie and P. J. Diamessis, "The internal gravity wave field emitted by a stably stratified turbulent wake," J. Fluid Mech. **720**, 104–139 (2013).
[4] B. R. Sutherland and P. F. Linden, "Internal wave generation by flow over a thin barrier," J. Fluid Mech. **377**, 223–252 (1998).
[5] D. A. Aguilar and B. R. Sutherland, "Internal wave generation from rough topography," Phys. Fluids **18**, 066603 (2006).
[6] H. A. Clark and B. R. Sutherland, "Schlieren measurements of internal waves in non-Boussinesq fluids," Exp. Fluids **47**, 183–190 (2009).
[7] P. F. Linden, "The deepening of a mixed layer in a stratified fluid," J. Fluid Mech. **71**, 385–405 (1975).
[8] K. Dohan and B. R. Sutherland, "Numerical and laboratory generation of internal waves from turbulence," Dyn. Atmos. Oceans **40**, 43–56 (2005).
[9] J. K. Ansong and B. R. Sutherland, "Internal gravity waves generated by convective plumes," J. Fluid Mech. **648**, 405–434 (2010).
[10] D. D. Sentman, E. M. Wescott, R. H. Picard, J. R. Winick, H. C. Stenbaek-Nielsen, E. M. Dewan, D. R. Moudry, F. T. S. Sabbas, M. J. Heavner, and J. Morrill, "Simultaneous observations of mesospheric gravity waves and sprites generated by a midwestern thunderstorm," J. Atmos. Solar-Terr. Phys. **65**, 537–550 (2003).
[11] B. R. Sutherland and W. R. Peltier, "Turbulence transition and internal wave generation in density stratified jets," Phys. Fluids A **6**, 1267–1284 (1994).
[12] B. R. Sutherland, "The dynamic excitation of internal gravity waves in the equatorial oceans," J. Phys. Oceanogr. **26**, 2398–2419 (1996).
[13] B. R. Sutherland, "Rayleigh wave-internal wave coupling and internal wave generation above a model jet stream," J. Atmos. Sci. **63**, 1042–1055 (2006).
[14] H. T. Pham and S. Sarkar, "Internal waves and turbulence in a stable stratified jet," J. Fluid Mech. **648**, 297–324 (2010).
[15] J. R. Taylor and S. Sarkar, "Internal gravity waves generated by a turbulent bottom Eckman layer," J. Fluid Mech. **590**, 331–354 (2007).
[16] B. Gayen, S. Sarkar, and J. R. Taylor, "Large eddy simulation of a stratified boundary layer under an oscillatory current," J. Fluid Mech. **643**, 233–266 (2009).
[17] B. R. Sutherland, "Finite-amplitude internal wavepacket dispersion and breaking," J. Fluid Mech. **429**, 343–380 (2001).
[18] B. R. Sutherland, "Weakly nonlinear internal wavepackets," J. Fluid Mech. **569**, 249–258 (2006).
[19] H. Kato and O. M. Phillips, "On the penetration of a turbulent layer into stratified fluid," J. Fluid Mech. **37**, 643–655 (1969).
[20] G. Oster, "Density gradients," Sci. Am. **213**, 70 (1965).
[21] B. R. Sutherland, S. B. Dalziel, G. O. Hughes, and P. F. Linden, "Visualisation and measurement of internal waves by "synthetic schlieren". Part 1: Vertically oscillating cylinder," J. Fluid Mech. **390**, 93–126 (1999).
[22] S. B. Dalziel, M. Carr, J. K. Sveen, and P. A. Davies, "Simultaneous synthetic schlieren and PIV measurements for internal solitary waves," Meas. Sci. Technol. **18**, 533–547 (2007).
[23] T. H. Ellison and J. S. Turner, "Turbulent entrainment in stratified flows," J. Fluid Mech. **6**, 423–448 (1959).
[24] J. S. Turner, "The influence of molecular diffusivity on turbulent entrainment across a density interface," J. Fluid Mech. **33**, 639–656 (1968).
[25] X. E and E. J. Hopfinger, "On mixing across an interface in stably stratified fluid," J. Fluid Mech. **166**, 227–244 (1986).
[26] S. Narimousa and H. J. S. Fernando, "On the sheared density interface of an entraining stratified fluid," J. Fluid Mech. **174**, 1–22 (1987).
[27] H. J. S. Fernando, "Turbulent mixing in stratified fluids," Ann. Rev. Fluid Mech. **23**, 455–493 (1991).

[28] D. L. Boyer, P. A. Davies, and Y. Guo, "Mixing of a two-layer stratified fluid by a rotating disc," Fluid Dyn. Res. **21**, 381–401 (1997).
[29] A. Shravat, C. Cenedese, and C. P. Caulfield, "Entrainment and mixing dynamics of surface-stress-driven stratified flow in a cylinder," J. Fluid Mech. **691**, 498–517 (2012).
[30] A. Fincham and G. Delerce, "Advanced optimization of correlation imaging velocimetry algorithms," Expt. Fluids **29**, S013–S022 (2000).
[31] B. R. Sutherland, *Internal Gravity Waves* (Cambridge University Press, Cambridge, UK, 2010), p. 378.
[32] J. R. Taylor, "Numerical simulations of the stratified oceanic bottom boundary layer," Ph.D. thesis (University of California, San Diego, 2008).
[33] C. Wunsch and R. Ferrari, "Vertical mixing, energy, and the general circulation of the oceans," Annu. Rev. Fluid Mech. **36**, 281–314 (2004).